48TH TURBOMACHINERY & 35TH PUMP SYMPOSIA
HOUSTON, TEXAS | SEPTEMBER 9-12, 2019
GEORGE R. BROWN CONVENTION CENTER

# NUMERICAL AND EXPERIMENTAL ANALYSIS OF FLOW-INDUCED SUBSYNCHRONOUS VIBRATIONS IN INTEGRALLY GEARED TURBOEXPANDERS

**Leonardo Baldassarre**
Engineering Executive for Centrifugal Compressors, Turboexpanders and Auxiliary Systems
BHGE
Florence, Italy

**Andrea Bernocchi**
Senior Engineering Manager for Centrifugal Compressors, Turboexpanders and Auxiliary Systems
BHGE
Florence, Italy

**Michele Fontana**
Engineering Manager for Centrifugal Compressors and Turboexpanders
BHGE
Florence, Italy

**Lorenzo Querini**
Turboexpander Design Engineer
BHGE
Florence, Italy.

**Davide Biliotti**
Aerodynamics Lead Engineer
BHGE
Florence, Italy.

**Ravi S.V. (Ravi Shanmugam Venkatachalam)**
Aerodynamics Lead Engineer
BHGE
Bengaluru, KA, India.

*Leonardo Baldassarre is currently Engineering Executive Manager for Compressors and Turboexpanders with BHGE in Florence, Italy. He is responsible for requisition, standardization and new product introduction for compressors, turboexpanders and auxiliary systems.*
*Dr. Baldassarre began his career with GE in 1997. He worked as Design Engineer, R&D Team Leader, Product Leader and Requisition Manager for centrifugal compressors. Dr. Baldassarre received a B.S. degree (Mechanical Engineering, 1993) and Ph.D. degree (Turbomachinery Fluid Dynamics, 1998) from the University of Florence. He authored or coauthored 20+ papers, mostly in the area of fluid dynamics and rotordynamics. He holds 5 patents.*

*Andrea Bernocchi is currently Senior Engineering Manager at BHGE in Florence, Italy. He joined GE in 1996 as Centrifugal Compressor Design Engineer after an experience in plastic machinery industry. He has 18 years of experience in design development, production and operation of centrifugal compressor. He covered the role of LNG compressor design manager for 6 years with responsibility in design of LNG compressors, testing and supporting plant startup. He's currently leading the requisition team for centrifugal and axial compressor design.*
*Mr. Bernocchi received a B.S. degree in Mechanical Engineering from University of Florence in 1994. He holds 4 patents in compressor field.*

*Davide Biliotti received the degree in Mechanical Engineering at the Department of Industrial Engineering of the University of Florence (Italy) in 2010. In the December 2013 he completed his doctorate in Energy and Innovative Industrial and Environmental Technology. His PhD project, conducted in collaboration with GE Oil & Gas, was based on the analysis of the rotating stall phenomenon in centrifugal compressors by means of experimental and numerical approaches. Starting from late 2013, he is working as Aerodynamic Lead Design Engineer for compressors and turboexpanders in BHGE. He authored or coauthored 15+ papers, mainly in the area of fluid dynamics.*

*Michele Fontana is currently Engineering Manager for Centrifugal Compressors and Turboexpanders at BHGE in Florence, Italy. He supervises the calculation activities related to centrifugal compressor design and testing, and has specialized in the areas of rotordynamic design and vibration data analysis.*
*Mr. Fontana graduated in Mechanical Engineering at University of Genova in 2001. He joined GE in 2004 as Centrifugal Compressor Design Engineer, after an experience in the automotive sector. He authored 10+ technical papers about rotordynamics and vibration monitoring, and holds two patents in this same field.*

*Lorenzo Querini is a Turboexpander Lead mechanical design engineer with BHGE. His responsibilities include the development of Turboexpander design, support to test and manufacturing activities as well as RCA for troubleshooting at site. Mr. Querini received a B.S. degree in Mechanical Engineering from University of Florence (Italy) in 2011. He joined BHGE as Turboexpander design Engineer in 2011 as well.*

*Ravi is an Aerodynamics Lead engineer in New Product Introduction group at BHGE. His responsibility includes radial turbomachinery aerodynamic design, aeromechanics modelling and analysis. He received his M.Eng. degree in Thermal Engineering from Anna University, Chennai, India, in 2000. He joined GE Appliance business in 2006 and moved to BHGE in 2008 and working on centrifugal compressor and radial expander aerodynamic design.*


## ABSTRACT

Turboexpanders are widely used as energy recovery systems, in plants where a stream of pressurized gas is available as output of the main process. In this kind of application the train layout is typically composed of a single or multi-stage radial inflow turbine, coupled with an electrical generator by means of a gearbox. The process gas flowrate is commonly controlled by acting on a set of adjustable Inlet Guide Vanes (IGV) positioned upstream of the expander wheel.
When a turboexpander is operated in off-design conditions at low load (typically during startup/shutdown transients), the tangential velocity of the discharge gas is high with respect to its axial velocity. In this condition the decelerated, swirled flow can generate a helical vortex in the diffuser, resulting in a pressure gradient of the core flow rotating around the diffuser axis. This rotating pressure gradient may induce radial rotor vibration.
The present study starts with an analytical description of this flow-generated vibration mechanism and a review of the results of dedicated numerical simulations and experimental tests. The characterization of the phenomenon is followed by the description of mitigating actions that can be carried out during the design phase to optimize the geometry and the operation of the turboexpander. Finally, the analysis of some case studies coming from OEM field experience provides evidence of how the vibration can be reduced through such mitigating actions.
This extensive theoretical and experimental analysis allows the engineer to draw some general conclusions and guidelines for the design and operation of turboexpanders, as well as to identify and minimize the risk of high vibrations due to vortex flow.


## INTRODUCTION

This study addresses expander-generator (EG) trains composed by a synchronous electrical generator coupled with an integrally-geared turboexpander, featuring one or more stages. Each expander stage includes a high-speed rotor (HSR) with a wheel assembled in overhung configuration on a geared shaft. Torque is transmitted by the HSR through the gear, to a low-speed rotor (LSR) that is connected to the generator by a flexible coupling. The gearbox is present in the majority of EG application, because normally the running speed of the expander stage(s) that maximizes the efficiency of the machine is higher than the running speed of the generator, that is fixed by the electrical grid frequency and by the number of generator poles.
A typical arrangement of an EG train is presented in Figure 1, while Figure 2 shows the gearbox in detail.
The main components of an expander stage are shown in Figure 3 and 4 and are described here below. The same part nomenclature is used in the rest of this study.

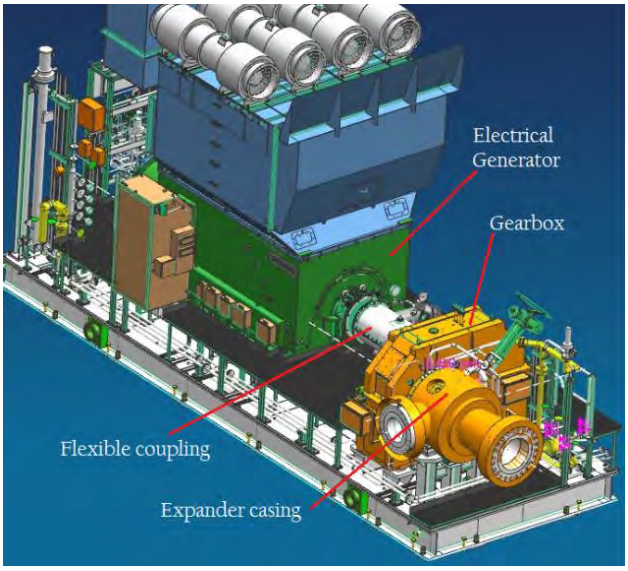


*Figure 1. General layout of an Expander Generator turbomachine.*

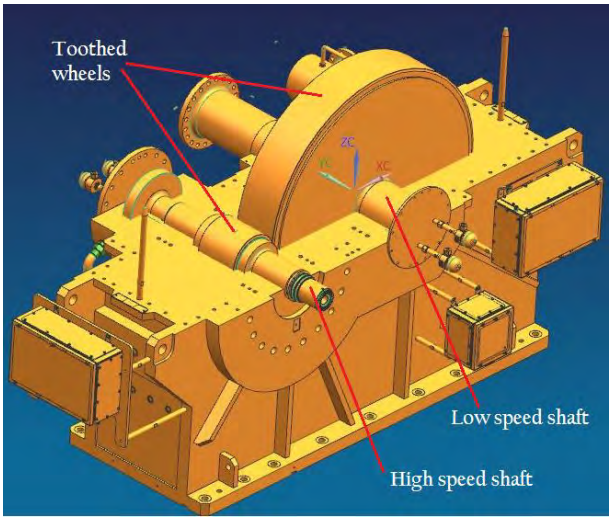


*Figure 2. General layout of an Expander Generator gearbox.*

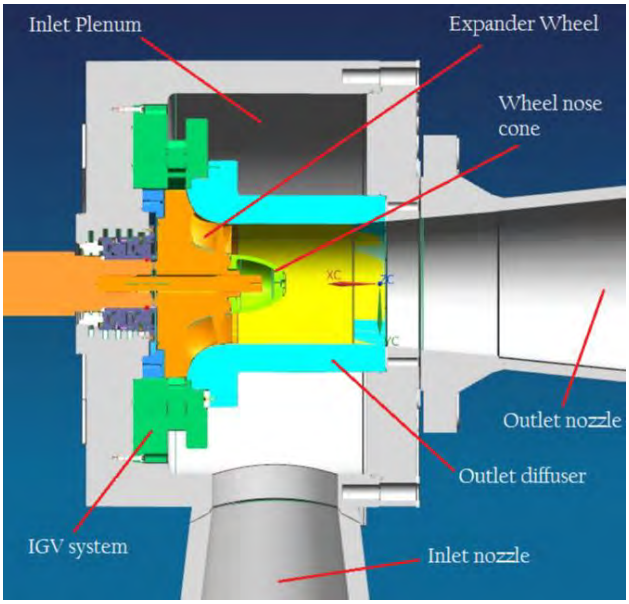


*Figure 3. General cross section of an Expander Generator.*

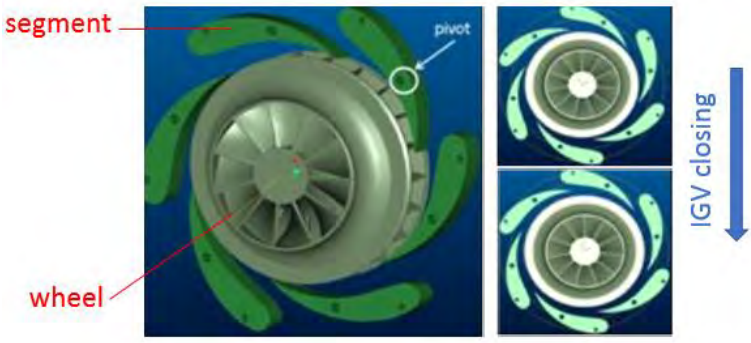


*Figure 4. Expander IGV system general layout*

*Inlet nozzle:* Flanged section that connects the EG casing to the process line, guiding the gas flow inside the machine.

*Inlet plenum*: Stator cavity used to slow down the gas coming from the inlet nozzle and to distribute its flow along the circumferential inlet section of the main expansion section.

*IGV system*: Adjustable inlet guide vanes (IGV) are used to control the power produced by the turboexpander. The IGV system includes a set of movable nozzle segments, the IGV actuator and the mechanical system used to transfer the motion from the actuator to the segments. This motion results in a variation of the inlet flow passage area, as shown in Figure 4. The thermodynamic function of the IGV's is to convert a portion of the total pressure of the gas into velocity, to optimize the inlet conditions at expander wheel.

*Wheel*: Extracts energy from the gas flow, converting it into mechanical torque that is transferred through the gearbox to the electric generator. Such energy extraction is done by reducing as much as possible the angular momentum of the gas entering the wheel; ideally the gas at wheel exit should have a purely axial velocity.

*Diffuser*: Tapered piping section located downstream of the wheel. Its increasing cross-section causes a deceleration of the gas flow,

and therefore - for a given static pressure downstream of the machine - a reduction of the gas static pressure at the wheel outlet. This allows the extraction of an additional fraction of the gas energy, therefore increasing the overall efficiency of the expander.

*Outlet nozzle*: This component connects the EG casing to the process line downstream of the expander, guiding the gas out of the machine.

Turboexpanders are commonly required to operate at low gas flowrate with respect to their design condition, for transient periods (typically startup and shutdown) and possibly also in stationary conditions, to match the variability of the available process gas stream. While expander-compressors can reduce their running speed in response to a lower gas flowrate, expander-generators do not have this degree of freedom, since the electrical generator imposes a fixed running speed. This means that the wheel of an EG running at low flowrate can operate in strongly off-design condition, with very high discharge flow swirl (the ratio between tangential and axial velocity of the gas). In this condition the gas flow can generate a helical vortex in the diffuser (Cassidy and Falvey, 1970) and an associated pressure gradient of the core flow rotating around the diffuser axis. The rotation frequency of this pressure gradient is normally between 0.3 and 0.6 times the rotating speed. This phenomenon is commonly referred to as *vortex flow*, and its occurrence on turboexpanders is already documented in literature (Hirata et al., 2017; Nishi et al., 2007; Zhang et al., 2010). It represents a flow-generated instability, since the rotating pressure gradient generates a net radial force on the rotor that therefore a subsynchronous rotor vibration, as shown in Figure 5. If the flow pressure gradient is high, or the rotor is highly sensitive to this excitation (e.g. if the vortex flow frequency is close to a natural frequency of the rotor system), the subsynchronous vibration level can prevent the operation of the machine.

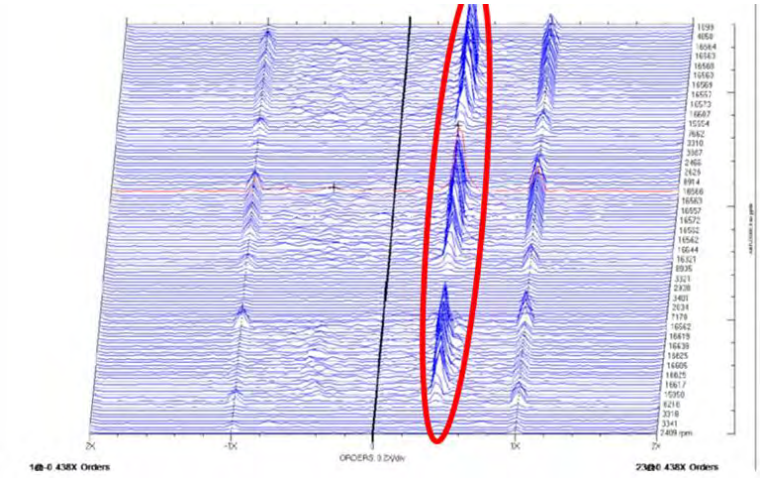

*Figure 5. Waterfall plot of a radial vibration probe, showing the subsynchronous vibration peak caused by vortex flow (highlighted in red), at ~40 percent of running speed frequency.*

A physical vortex model is adopted to describe this flow unsteadiness in the outlet diffuser. For a swirling flow in a conical diffuser, the tangential velocity distribution can be approximated by the Rankine-vortex model, i.e. a viscous inner core region surrounded by an effectively inviscid outer region. This results in a differential tangential velocity distribution, represented in Figure 6:

- Gas tangential velocity is directly proportional to radial distance from rotation axis ($c_{2u} \propto r$) for $r < R_{core}$.
- Gas tangential velocity is inversely proportional to radial distance from rotation axis ($c_{2u} \propto {}^{1}/_{r}$) for $r > R_{core}$, according to the free vortex model.

Therefore the Rankine vortex can be described as follows:

$$c_{2u}(r) = \begin{cases} \dfrac{\Gamma r}{2\pi R^2} & if\ r < R_{core} \\ \dfrac{\Gamma}{2\pi r} & if\ r > R_{core} \end{cases} \quad (1)$$

Where for an arbitrary closed loop $C$ in a fluid flow, the circulation $\Gamma$ is defined as:

$$\Gamma = \oint_c u \cdot ds \quad (2)$$

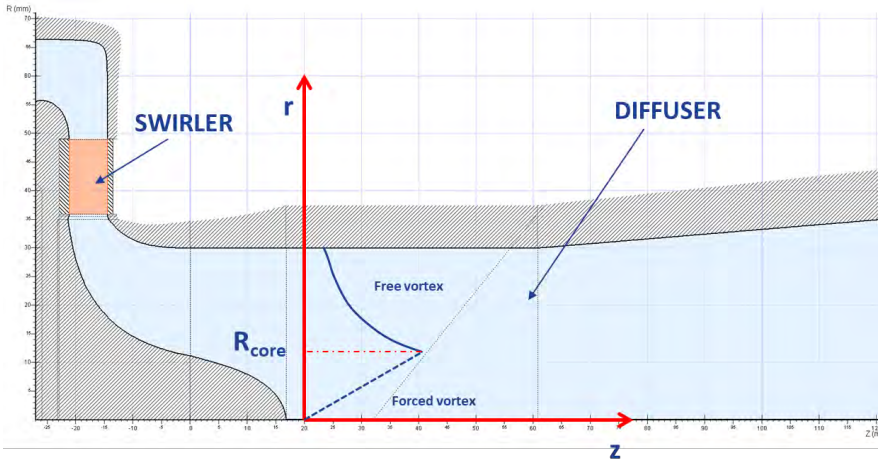


*Figure 6. Rankine vortex model for tangential velocity in a conical diffuser.*

A CFD analysis (see Appendix A) was performed on an existing EG geometry, to identify the gas recirculation zone downstream of the wheel nose (Figure 7) and the vortex formation predicted by theory (Figure 8).


*Figure 7. CFD output: cross-section of wheel and diffuser.*

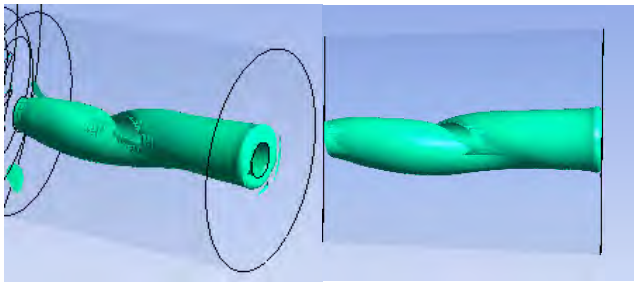

*Figure 8. CFD output: 3D view of the gas vortex in the diffuser.*

Following this theoretical analysis, an experimental campaign was carried out to characterize the phenomenon. The typical operating conditions of a turboexpander operating at partial load were reproduced with the aid of a simplified model test setup. The setup includes a fixed, vaned inlet section (nozzles) in place of the expander wheel, to provide the gas swirl at diffuser inlet (see Figure 9).

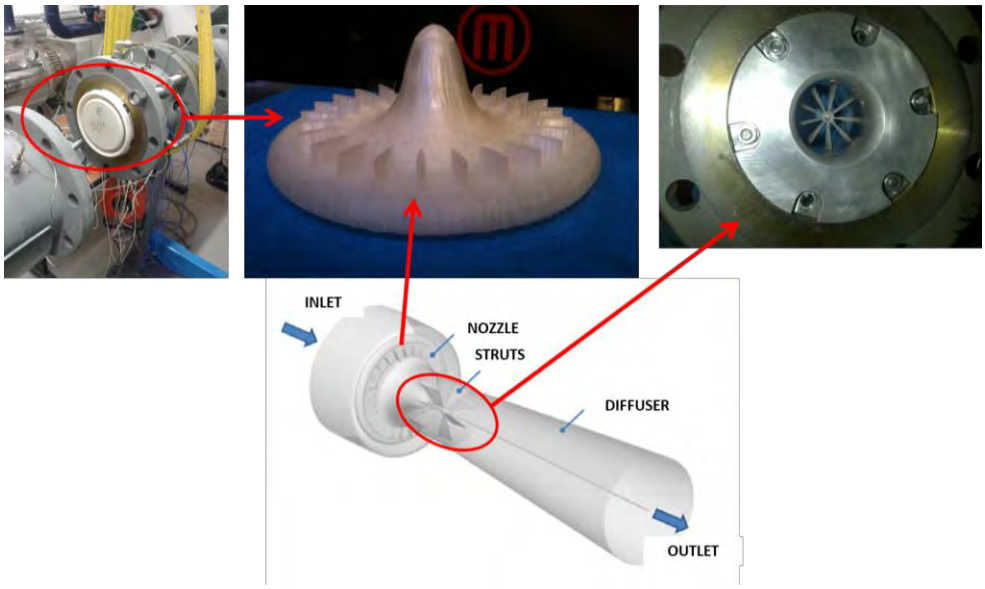


*Figure 9. Model test setup.*

Dynamic pressure probes were positioned along the diffuser to measure the pressure and frequency oscillations associated with the vortex flow phenomenon. The test was carried out in open loop, using an external blower to supply the air flow to the inlet plenum. Tests were run for several inlet swirl conditions, by using five different sets of inlet nozzles designed with different metal angles. Inlet pressure varied from 1.1 bar to 1.6 bar while the discharge was always at ambient conditions.
In the second part of the experiment a set of swirl breaks (struts) was applied to reduce the vortex formation. The struts are in a section at the diffuser inlet and consist of radial stator vanes designed with NACA profile (Abbott et al., 1945). Two different struts positions were tested, as shown in Figure 10. One close to the hypothetical wheel exit (A) and the other at the inlet of the conical diffuser (B). Finally, different inlet pressures (i.e. different mass flowrates) were tested to understand the effect on the vortex flow phenomenon.

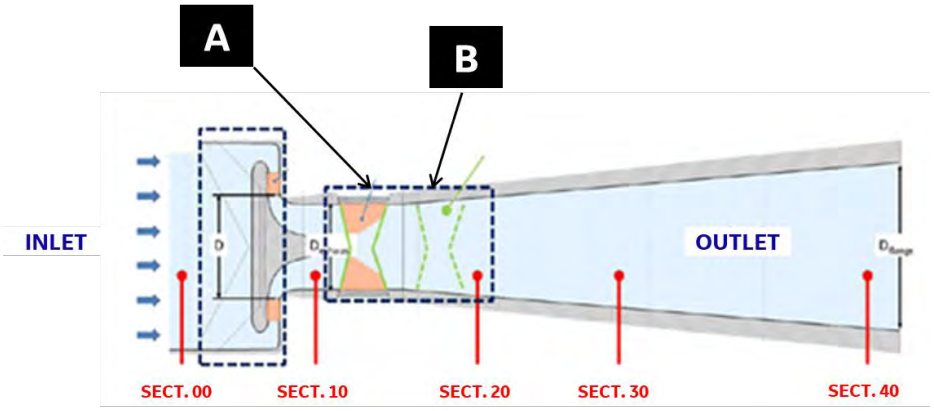


*Figure 10. Model test arrangement. The measurement sections are shown in red.*

The main results for the diffuser without struts are reported in Figure 11-12. The nozzle position parameter is the angle between the nozzle chord and the radial direction, therefore zero degrees corresponds to purely radial flow.
Figure 11 shows that, starting from 30 degrees nozzle position, a sharp frequency peak appears at 1100 Hz. This is a confirmation of the relation between inlet flow swirl and vortex flow formation in the diffuser.
Figure 12 highlights the effect of an inlet pressure variation on the frequency peak. The plot shows an approximately linear relation between the peak frequency and the inlet pressure.

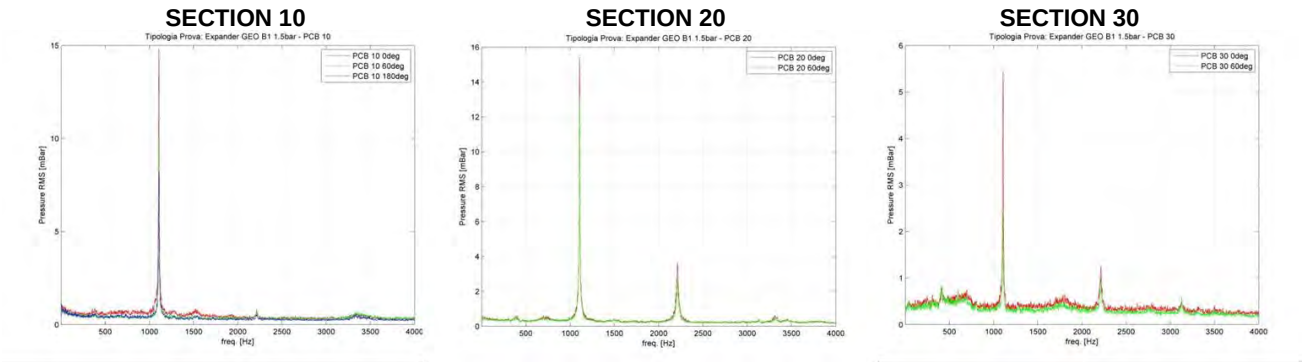


*Figure 11. FFT at Sections 10, 20 and 30 for 30 degree nozzle position.*

The results are summarized by using a swirl parameter, defined in Equation (3) according to literature (Tse, 2004; Wood et al., 2010; Powell, 1964). A factor $K_{2u}$ is used to quantify the tangential momentum at diffuser inlet, see Equation (4). Since in this test no rotating wheel is present, Equation (4) is reduced to the simplified expression of Equation (5). When the wheel is present, the correct expression for $K_{2u}$ is the one reported in Equation (6).
Another useful parameter to quantify the vortex flow phenomenon is the Strouhal number, defined in Equation (7).

$$\Omega = \frac{K_{2u} D_2}{\rho_2 {Q_2}^2} \tag{3}$$

$$K_{2u} = \int c_{2u} r_2 d\dot{m} \tag{4}$$

$$K_{2u} = \dot{m} u_1 \frac{D}{2} \tag{5}$$

$$K_{2u} = \dot{m} u_1 \frac{D_1}{2} S_2 \qquad with \qquad S_2 = \frac{c_{1u}}{u_1} - \frac{W}{\dot{m} u_1^2} \tag{6}$$

$$Sh = \frac{f {D_{2s}}^3}{Q_2} \tag{7}$$

where:
$D_1$ is the outer wheel diameter [m]
$u_1$ is the wheel peripheral speed measured at diameter $D_1$ [m/s]
$D_2$ is the inlet diffuser diameter [m]
$D_{2s}$ is the diameter at the shroud of the wheel outlet, here considered equal to $D_2$ [m]
$\rho_2$ is the gas density at the diffuser inlet [kg/m$^3$]
$Q_2$ is the volume flowrate at diffuser inlet [m$^3$/s]
$\dot{m}$ is the mass flowrate [kg/s]
$c_{1u}$ is the tangential velocity at the wheel inlet [m/s]
$c_{2u}$ is the tangential velocity at the wheel outlet [m/s]
$f$ is the vortex frequency [Hz]

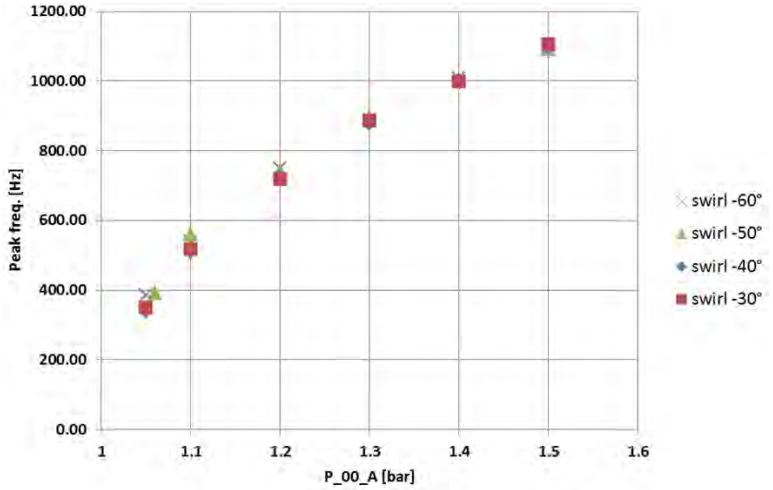


*Figure 12. Peak frequency vs. inlet pressure for diffuser without struts.*

The overall results are reported in Figure 13, together with data from literature (Falvey et al., 1970) and data measured on an actual expander-generator running at site, that is presented in the Case Study section of this paper.
The good agreement between model test and site data confirms the strong correlation between rotor vibrations and the aerodynamic force induced by vortex flow.
Figure 14 shows a comparison among all the tested configurations, in terms of frequency spectrum of pressure measurements at diffuser inlet (i.e. at Section 10). The 1100 Hz frequency completely disappears in configuration *A*. In addition, a new frequency with a lower amplitude appears at 3300 Hz, highlighting a variation of the unsteady phenomenon. In configuration *B* no peak frequency associated to vortex flow is detected.

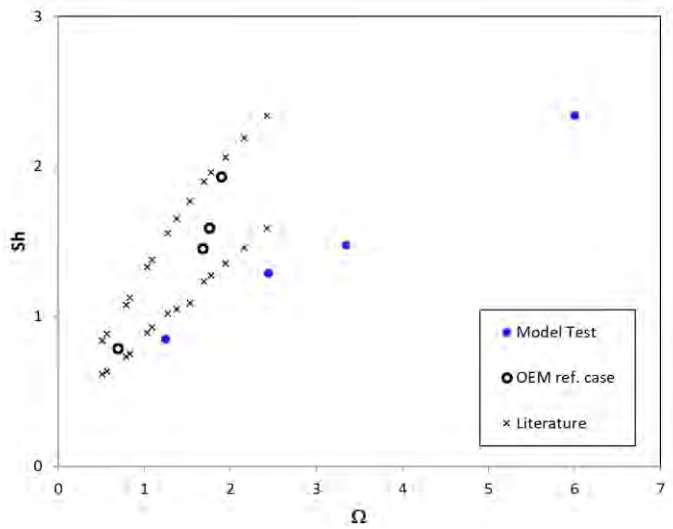


*Figure 13 – Summary results.*

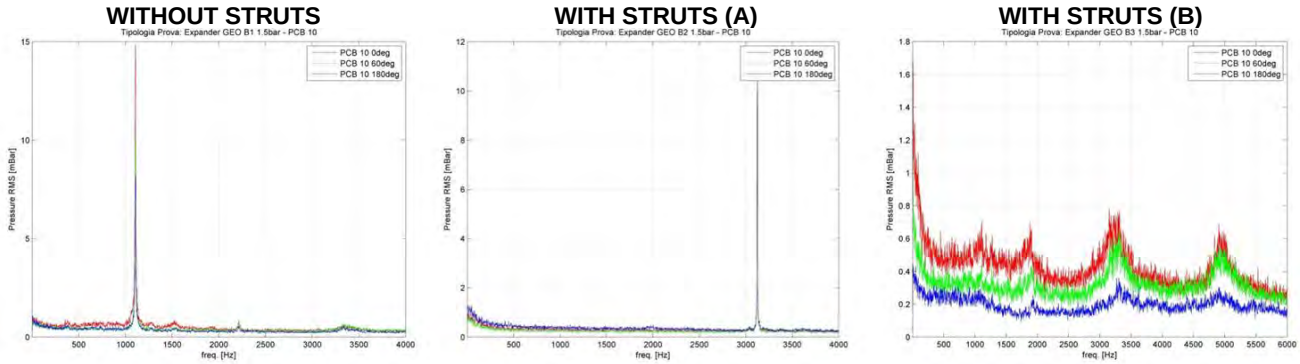


*Figure 14. FFT at Section 10 for different diffuser configurations, at -30 degree nozzle position.*

## MITIGATION METHODS

The risk of high rotor vibrations due to vortex flow excitation can be addressed by reducing the magnitude of the aerodynamic phenomenon and/or by reducing the sensitivity of the rotor system to this excitation.
Some possible mitigation methods are reviewed in the next paragraphs. Most of them were applied on the expander-generators presented as case studies for this paper, and their effects are discussed in detail in a dedicated section of this study.

***1. Minimize the swirl factor***

Experimental analyses of the vortex flow phenomenon (Falvey and Cassidy, 1970) show that the subsynchronous vibration amplitude is roughly proportional to the swirl number $\Omega$, that in turn is proportional to the Strouhal number *Sh*. This was also confirmed by data analyses carried out for the present study, as shown in Figure 13 and 27 to 30.
The formulation of the swirl number $\Omega$, derived from Equations (3) and (6), is the following:

$$\Omega = \frac{D_1 D_2}{2Q_2}\left(c_{1u} - \frac{W}{\dot{m}u_1}\right) \tag{8}$$

The parameters $Q_2$, $\dot{m}$ and $W$ (i.e. volume flowrate, mass flowrate and generated power) are considered as input conditions that cannot be varied. The swirl factor approaches zero when the sum of the two terms in parenthesis approaches zero; this normally corresponds to the design condition of the expander, where the absolute velocity of the gas at wheel discharge has little or no tangential component. However, in off-design conditions (i.e. low load), the term in parenthesis increases. The swirl factor can also be minimized by reducing the factor $D_1D_2$, but this is subject to design constraints:

- The wheel outer diameter $D_1$ and rotational speed ($N$) are selected as a function of input process data (gas volume flowrate $Q_2$, isentropic enthalpy drop $\Delta h_{is}$ through the expansion) aiming to optimize the efficiency (Bloch, 2001). Moreover the selection of $D_1$ is constrained upwards by the mechanical stress generated on the wheel by centrifugal force. Therefore reducing $D_1$ is not the best way to avoid vortex flow vibration issues, since it is not a free parameter.

- Modify the wheel eye diameter $D_2$. For given input process data, once that $N$ and $D_1$ are defined, the wheel exit diameters $D_{2s}$ and $D_{2h}$ are selected based on several criteria. $D_{2h}$ shall be large enough to allow the fitting of the tie rod (visible in Figure 3), whose size depends on the size of the rotor and its transmitted power. $D_{2s}$ shall be optimized for performance reasons: the smaller it is, the smaller the wheel exit passage section and the higher the gas velocity $c$. The larger it is, the larger the peripheral speed $u_2$. Efficiency is negatively affected by both high $c$ and $u_2$; therefore there is an optimum range for $D_{2s}$ that maximizes efficiency. Moreover there are other constraints reported in literature. According to (Rohlik, 1968) the relation $D_{2s} / D_1 \leq 0.7$ shall be satisfied to avoid excessive shroud curvature, while the ratio $D_{2h} / D_{2s}$ shall be equal or higher than 0.4, to avoid excessive hub blade blockage and energy loss (Kun and Sentz, 1988 provide a slightly lower limit of 0.35). In addition there are structural and manufacturability constraints. A large ratio $D_{2s} / D_{2h}$ may lead to a blade geometry that is weak from a structural standpoint and difficult to manufacture by machining due to poor accessibility of the vanes.

- Reduce the tangential component of the gas velocity at wheel inlet, $c_{1u}$. The magnitude of $c_{1u}$ is defined by the shape and position of the IGV's that are used as main control system of the machine. The IGV exit angle is defined during the design phase to maximize the efficiency (Fiaschi et al., 2015). The IGV position can be optimized during transients to reduce the subsynchronous vibration amplitude, as discussed at point 6 below.

- Increase the speed $u_1$. This is normally constrained by mechanical stress of the wheel. Since the mechanical stress is mainly due to centrifugal forces, open-blade wheels can withstand higher peripheral speed than closed wheels and aluminum or titanium alloy wheels can withstand higher peripheral speed than steel wheels.

***2. Design a subcritical rotor***

The amplitude of subsynchronous vibration induced by vortex flow is strongly increased if its frequency gets close to a critical speed of the rotor+bearing system. In absence of specific constraints it is relatively common for the HSR of a turboexpander-generator to operate above its first critical speed, but an effective option to minimize the risk of vortex flow vibrations is to design a stiff rotor+bearing system with the first critical speed above the operating speed range. Normally this is done by reducing as much as possible the mass, bearing span and total length of the rotor and by increasing the stiffness of the journal bearings.

***3. Install stator vanes on the diffuser***

An effective way to act on the exciting source is to apply stator vanes (struts) in the diffuser. Such planar elements, parallel to the diffuser meridional section, straighten the gas flow and strongly reduce the discharge gas recirculation. The downside is that they represent an additional cost and an increase of design complexity. They must be designed to avoid resonances and coincidence with the vibration modes of the wheel. If the aerodynamic design of the struts is properly done, the efficiency loss due to the resistance to the gas flow is negligible.

***4. Optimize the geometry of the wheel***

Besides the optimization of the inlet and exit diameters discussed in point 1, there are other design features of the wheel that have a direct effect on the subsynchronous vibration amplitude. The wheel geometry influences the formation of the rotating pressure gradients associated to vortex flow, and it also determines the sensitivity of rotor vibrations to the aerodynamic excitation. For example, the vibration induced on a closed wheel by a given pressure gradient is normally higher than for an open wheel, since the closed wheel has more surface exposed to a differential pressure. Another important feature is the shape of the wheel downstream of the trailing edge of the blades. It can be an ogival or conical nose, as in Figure 2 and 3, a flat surface, or even just the exposed end of the wheel tie rod and wheel retaining nut. This geometry influences the shape of the discharge gas flow path and recirculation volume, which influences the vortex flow mechanism and the pressure gradient formation. Additionally it has a passive role, since - for a given pressure fluctuation - its meridional cross-sectional area is proportional to the net radial force acting on it.

***5. Increase the stiffness of the rotor + journal bearings system***

The sensitivity of rotor radial vibrations to vortex flow excitation can be reduced by increasing the stiffness of the system, even if a subcritical condition as described at point 2 cannot be achieved. Increasing the stiffness of the system reduces its sensitivity (in terms of vibration amplitude) to a mechanical excitation. This stiffness increase is normally achieved by designing a rotor with shorter overhung sections and larger shaft diameter and by reducing the clearance of the journal bearings. The main limiting factors are related to layout requirements and to the safe operation of the bearings themselves. Higher diameter and lower clearance result in higher pad temperature that may lead to wear and failure.

***6. Optimize control parameters (IGV and process gas valves opening)***

Expander inlet flowrate is controlled by adjusting the opening of the IGV's located upstream of the wheel. In a typical arrangement (see Figure 4), closing the IGV's has the effect of increasing the tangential component of the gas velocity $c_{1u}$. As discussed above, this results in an increase of the swirl factor $\Omega$, that may lead to high subsynchronous vibration of the rotor.

One possible mitigating action is to develop a startup and loading procedure that maximizes the IGV opening. This can be done by acting on the process gas valve(s) located upstream of the expander. Normally there is a trip valve used only for machine protection, and another smaller bypass valve positioned in parallel to the trip valve. At startup, the trip valve is closed and the bypass valve is opened, to provide just the small gas flowrate needed for the breakaway of the machine and the ramp-up at rated speed. Once the breakers are closed and the expander-generator is running at no load, the trip valve is opened from 0 percent to 100 percent, with IGV set at minimum opening. Subsequently the IGV are slowly opened to increase the gas flowrate and therefore the power load. This procedure is critical for vortex flow, because there is a transient condition at low load where the minimum IGV opening results in a high value of $c_{1u}$. An alternative is to achieve the load increase by slowly increasing the flow through the trip valve, while keeping the IGV open. The downside is that this adds complexity to the control logic and the startup procedure, and that the trip valve often does not allow a sharp partial flow regulation.

## CASE STUDIES

Significant subsynchronous radial vibrations induced by vortex flow were detected during the commissioning phase of three EG trains. This section summarizes these field experiences, together with data comparison showing the effect of the mitigating action listed in the previous section.

The main geometrical data and operating parameters of the three case studies are listed in Table 2.

| | Unit A | Unit B | Unit C |
|---|---|---|---|
| Stage number | 2 | 1 | 1 |
| Wheel type | Closed | Open | Closed |
| Wheel diam [mm] | 465 (HP); 1000 (LP) | 467 | 340 |
| Mass flow [kg/h] | 400000 | 800000 | 130000 |
| Inlet pressure [bara] | 39.2 (HP); 8.2 (LP) | 78.1 | 37.5 |
| Outlet pressure [bara] | 8.3 (HP); 1.3 (LP) | 44.6 | 13.1 |
| Inlet Temperature [°C] | 250 (HP); 188 (LP) | -23.1 | -9 |
| Inlet Density [kg/mc] | 101 (HP); 188 (LP) | 99 | 34 |
| Gas Type | Cycloalkane | Natural Gas | CO + H2 + CO2 |
| Gas MW [kg/kmol] | 70 | 19 | 20 |
| Rated generated total power [kW] | 7200 (HP); 8900 (LP) | 7500 | 3100 |
| Wheel rated speed [rpm] | 10200 (HP); 4900 (LP) | 8000 | 16500 |

*Table 2. Main parameters of case study expander-generators.*

***UNIT A: Subsynchronous vibration as a function of operating parameters***

During the commissioning activities of this two-stage turboexpander, unexpected high radial vibrations were observed on both high-speed shafts. Overall vibration amplitude approached the alarm threshold. Vibrations were higher during the speed ramp-up phase, at no and partial load. Waterfall plots show a dominant synchronous component (1X) in the speed ramp-up step, and a dominant, sharp-peak subsynchronous component (at frequency 0.4X for HP stage and 0.55X for LP stage) during operation at partial loads, see Figures 15-16.

The subsynchronous vibration are mainly detected by the X-Y expander wheel side vibration probes, whereas the coupling side vibrations are much lower.

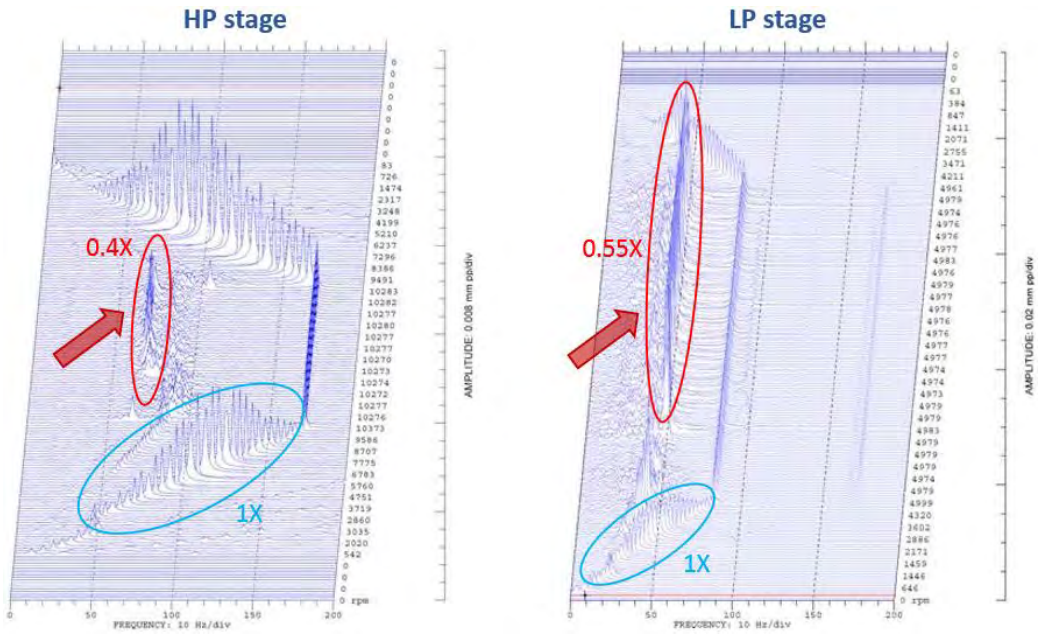


*Figure 15. HP and LP stage waterfall plots, showing dominant synchronous vibration during speed ramps and dominant subsynchronous vibration during operation at full speed and low load.*

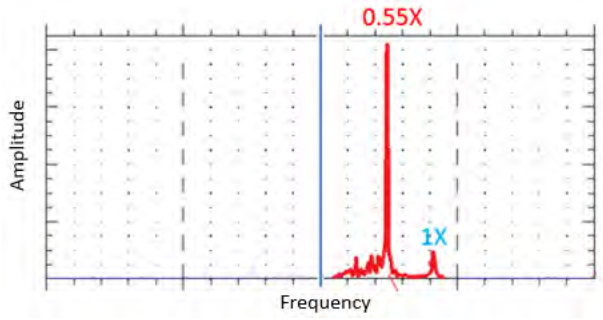


*Figure 16. LP stage radial vibration frequency spectrum, showing dominant sub synchronous vibration..*

Higher synchronous vibration during speed increase and no load operation is due to the relatively low stiffness of the journal bearings in those conditions, since the stiffness of oil-lubricated bearings increases with the radial load acting on them. On integrally geared units the HSR journal bearing load is the result of the rotor weight and the radial force transmitted by the gear; the latter is normally the largest component, and it is proportional to the gearbox transmitted torque and power. Therefore when the turboexpander is operating at low load the journal bearing load is also low.

The frequency of the subsynchronous vibration peak observed at low load (and therefore the calculated Strouhal number) is aligned with the vortex flow aerodynamic excitation theory, as shown later in Figures 29-30: the peak frequency is inversely proportional to the load. The amplitude of the subsynchronous vibration peak decreases when the power increases. This behavior is in line with expectations: when the mass flowrate through the expander wheel increases towards the design condition, the shape of the velocity triangle gets closer to the design condition and the outlet swirl angle of the gas is reduced.

Subsynchronous vibration amplitudes also shows a direct correlation with the unit discharge pressure (Figure 17). This trend, that is in agreement with the computational fluid dynamic analysis results, is due to the increase of the aerodynamical excitation on the rotor system due to the increase of the gas density.

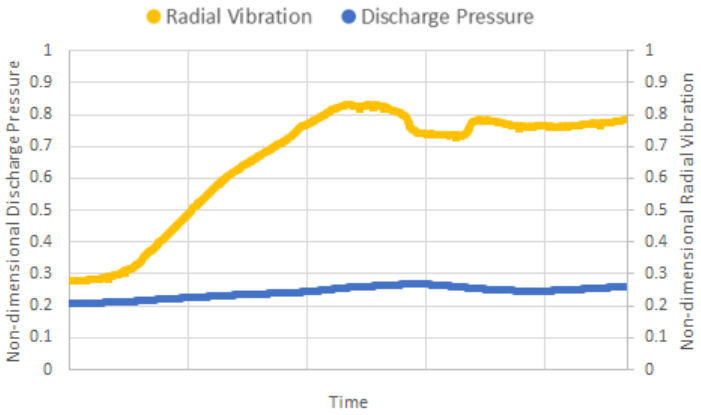


*Figure 17. LP rotor radial vibration and unit discharge pressure variation over time.*

Subsynchronous vibrations detected at partial load were significantly reduced by tuning the LP IGV's opening values.
The unit control logic adjusts the IGV opening of LP and HP stages based on the operating parameters (mainly on the pressure values upstream and downstream of each stage), to optimize the split of the total enthalpy drop between the two stages. Increasing the LP stage IGV opening position has the effect of reducing the back-pressure, thus increasing the HP stage head and reducing the LP stage head.
At partial load the increase of the LP stage IGV opening brings the gas absolute velocity inlet angle at expander wheel inlet closer to the design condition, see Figure 19. Getting closer to the design velocity triangle allows to reduce the outlet swirl angle and the correlated vortex flow generation.

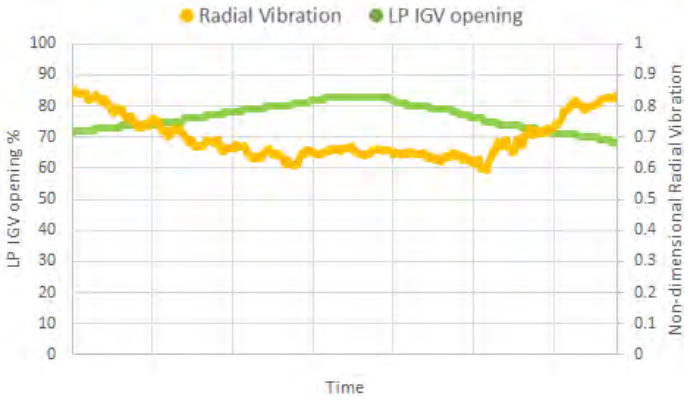


*Figure 18. LP rotor radial vibration in function of LP IGV opening over time.*

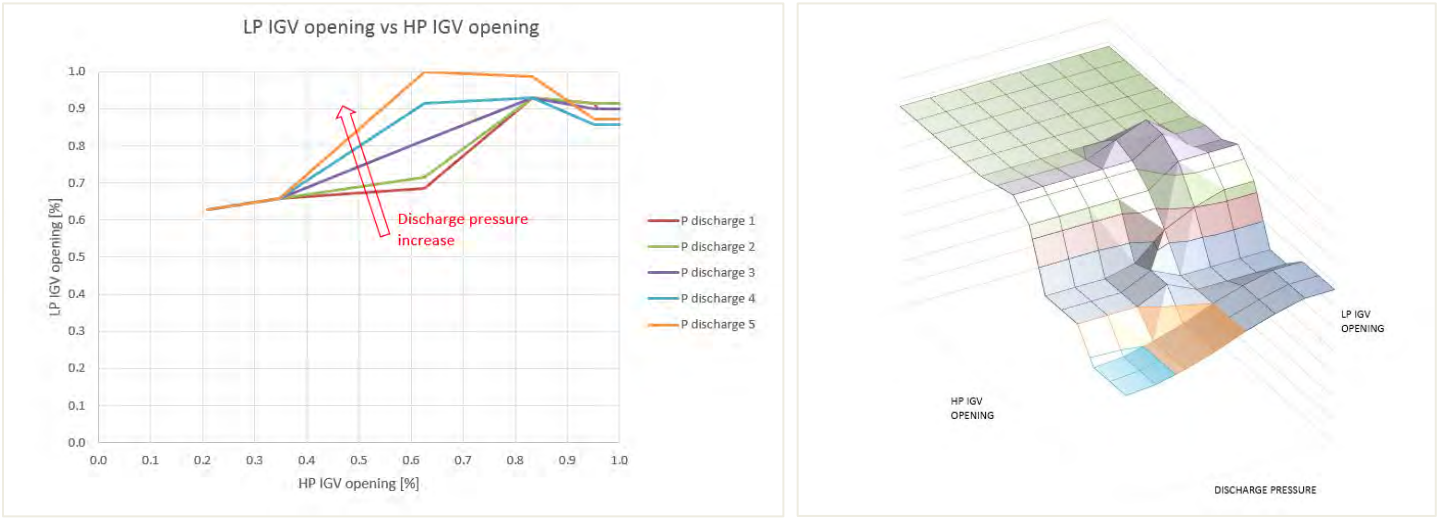


*Figure 19. LP IGV opening in function of HP IGV opening and unit discharge pressure*

***UNIT B: Subsynchronous vibration as a function of wheel geometry***

Reference Unit B highlighted a behavior similar to Unit A during the commissioning phase, with high overall radial vibration detected on the HSR expander side probes. High vibration occurred at partial load. The waterfall plots and frequency spectra show broadband subsynchronous vibration and dominant 1X component at very low load. Increasing the load has the effect of transforming the broadband subsynchronous vibration into a single, narrow frequency peak. During operation at rated speed, this peak frequency is function of the unit load.

The waterfall plot of Figure 20 shows broadband subsynchronous vibration at low load (bottom part of the plot, corresponding to operation at less than 30 percent of rated power). As the load was increased, a sharp vibration peak appeared at a distinct frequency (approx. 0.6X). When the generated power (load) was further increased, the frequency decreased down to about 0.4X.

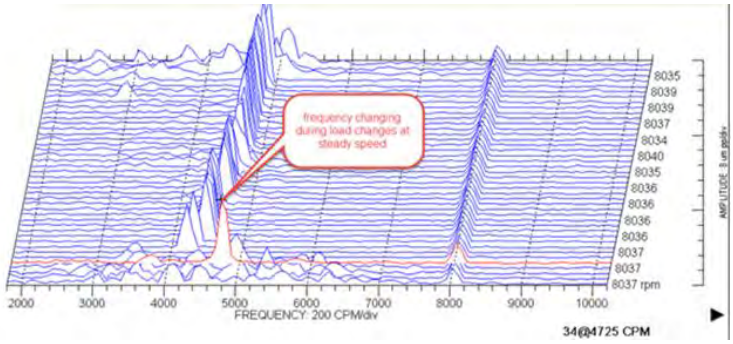


*Figure 20. Waterfall plot shows the sub synchronous vibration frequency variation basing on load.*

The subsynchronous vibration trend is clearly visible on the frequency spectra of Figure 21. The observed peak frequency is inversely proportional to the power generated, as predicted by theory and previously discussed for Unit A.

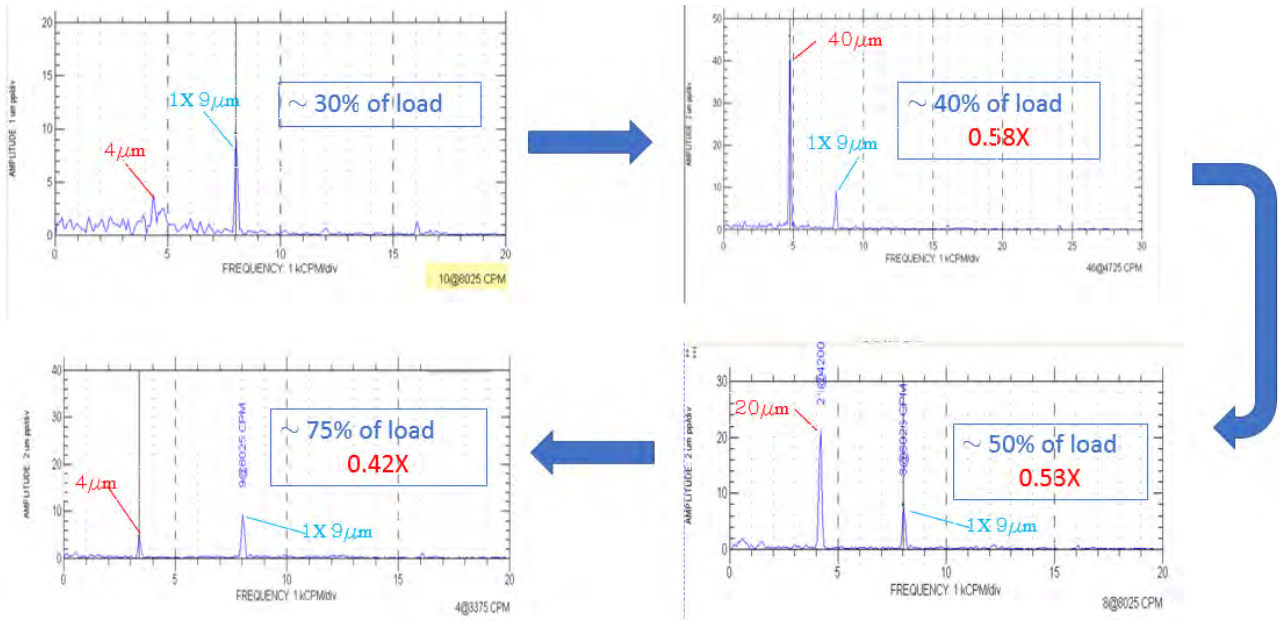


*Figure 21. Spectrum plots showing the subsynchronous vibration peak frequency and amplitude variation vs. load increase.*

The subsynchronous vibration at partial load was mitigated by reducing the rotor system sensitivity to the aerodynamic excitation generated by the vortex flow phenomenon. The wheel outlet geometry was modified by removing the wheel nose cone, which was identified as a potential contributor of the vibration phenomenon (see point 4 of Mitigation Methods section). The effect was a reduction of the overall radial vibration amplitude, by approximately 5% of the alarm threshold over the whole unit load range, compared with the previous runs performed with the nose cone: see Figure 22. More in detail, the comparison between the waterfall plots of expander side radial vibration for the two tested configurations shows a reduction of the subsynchronous vibration peak after the nose cone removal (see Figure 23). This is likely due to two factors: the first is the reduction of the rotor meridional cross-section at the expander

wheel discharge, i.e. the surface that is excited by the rotating pressure gradient associated to the vortex flow. The second factor is the reduction of the intensity of the rotating pressure gradient, associated to a reduction of the recirculation zone downstream of the wheel. This effect can be estimated by comparing CFD output plots similar to those shown in Figure 7-8, that are calculated for different geometries (with / without nose cone).

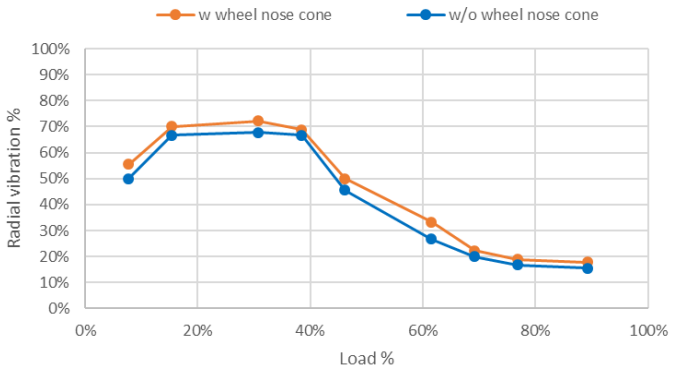


*Figure 22. Effect of the wheel nose cone removal on the radial vibrations, scaled by the alarm value, along all the power spectrum.*

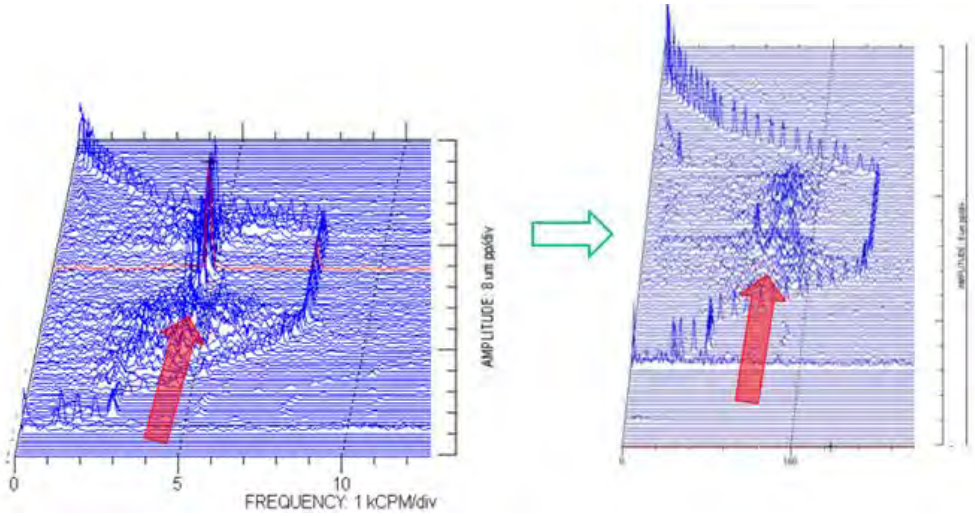


*Figure 23. Comparison of waterfall plots of the unit equipped with nose cone (left) and the unit without nose cone (right).*

***UNIT C: Effect of diffuser struts on subsynchronous vibration***

The behavior of reference Unit C during the commissioning phase shows clear similarities with the other two units. High overall radial vibration of the HSR was detected during operation at partial load, mainly on the expander side of the rotor.
In this unit the subsynchronous vibrations proved to be very sensitive to the IGV opening. This prevented the synchronization and loading of the unit while using the standard IGV opening values foreseen during the start-up sequence.
Tests were performed starting from fully open IGV position, and then reducing the opening while running the machine at rated speed. At some point the radial vibration increased steeply, see Figure 24.
Waterfall plots during load transients (Figure 25a) show a high subsynchronous peak at 0.4X to 0.5X of rotating frequency. The peak amplitude gets very high when the IGV opening position decreases below a threshold value, leading to unit trip for high vibrations. Figure 25a shows three subsequent startup attempts followed by trip.
To mitigate the phenomenon, the OEM studied an aerodynamic device in order to directly attenuate the excitation source.
The device consists of a stator group of radial vanes (also called *struts* or *vortex breakers*) installed in the outlet diffuser, with the principal goal to break the vortex flow and reduce the excitation of the rotor system (Figure 26).

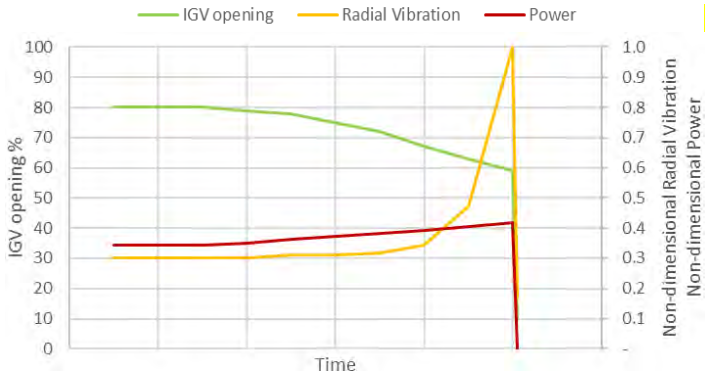


*Figure 24. Trends vs. time of IGV opening, turboexpander load and HSR radial vibrations. Vibration amplitude increases steeply while the IGV opening is gradually reduced.*

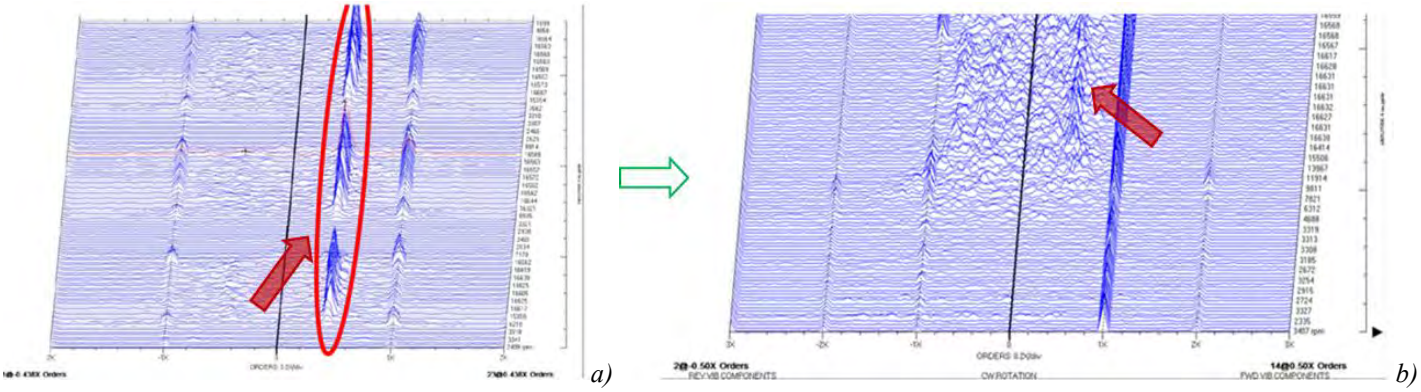


*Figure 25. Comparison of waterfall plots of unit C, (a) without struts during 3 start-up attempts, and (b) equipped with struts, during stable operation.*

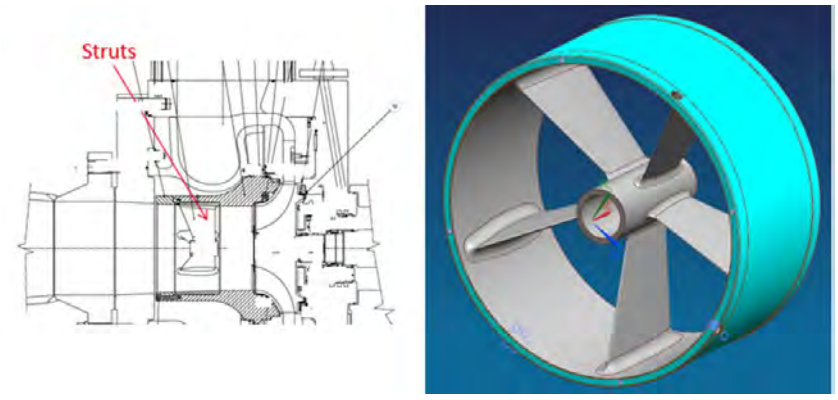


*Figure 26. Struts geometry and application zone inward the flow path.*

The vane geometry was optimized with the aid of CFD analysis, starting from a NACA profile to minimize the impact on expander efficiency and maximize the vortex breaking effect and the straightening of the outlet gas flow. This component was fabricated by additive manufacturing production technology, by means of a laser 3D printing system.

After the installation of the struts inside the machine, the unit showed a significant reduction of subsynchronous vibration amplitudes over the whole partial speed and partial load ranges with respect to the original configuration. Figure 25b shows a much lower subsynchronous peak vs. Figure 25a, even if the IGV position in Figure 25b is more unfavourable, i.e. IGV's are more closed, leading to higher gas swirl. (The scale of the vertical axis is different between the two plots, as visible from the height of 1X peak. The subsynchronous peak in Figure 25a is about three times higher than in Figure 25b).

***Summary of Case Studies results***

The site data of the three reference units highlight a good correlation with the literature, CFD and the experimental campaign performed on dedicated test bench. The results are regrouped in the following diagrams.
The overall radial vibration amplitude is roughly proportional to the swirl number defined in Equation (8), as shown in Figure 27.

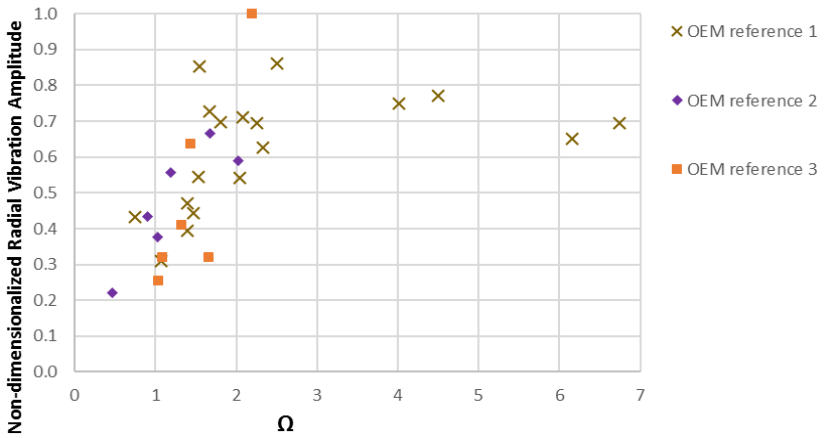


*Figure 27. Rotor radial vibration amplitude in function of the swirl number, for the three reference units.*

The subsynchronous vibration peak frequency is inversely proportional to the volumetric flow, that in turn is directly proportional to the unit load (generated power), as visible in Figure 28.

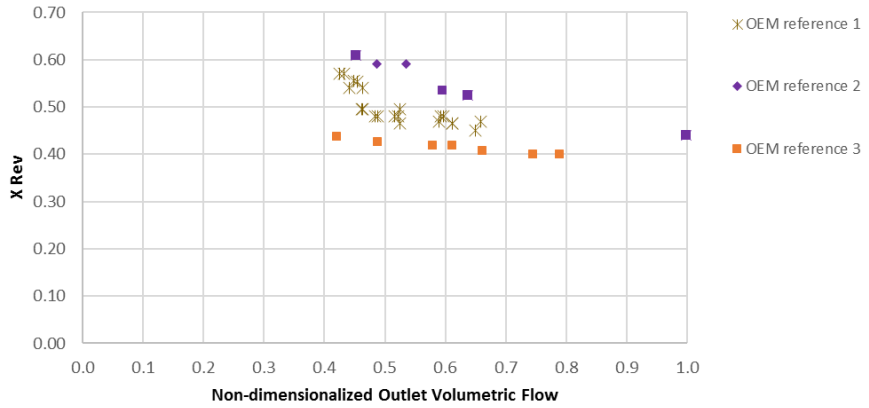


*Figure 28. Subsynchronous vibration frequency (X Rev) in function of the outlet volumetric flow, for the three reference units.*

The swirl number is inversely proportional to the unit load (Figure 29).

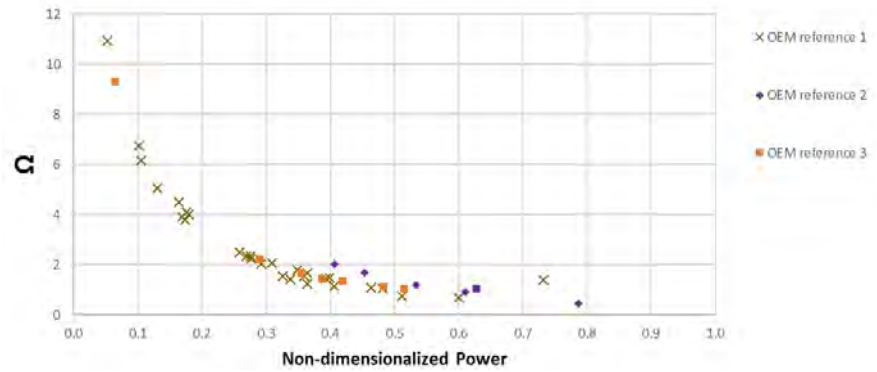


*Figure 29. Swirl number in function of load for the three reference units.*

The Strouhal number, that is directly proportional to the frequency of the subsynchronous vibration peak (see Equation 7), is directly proportional to the swirl number (Figure 30).

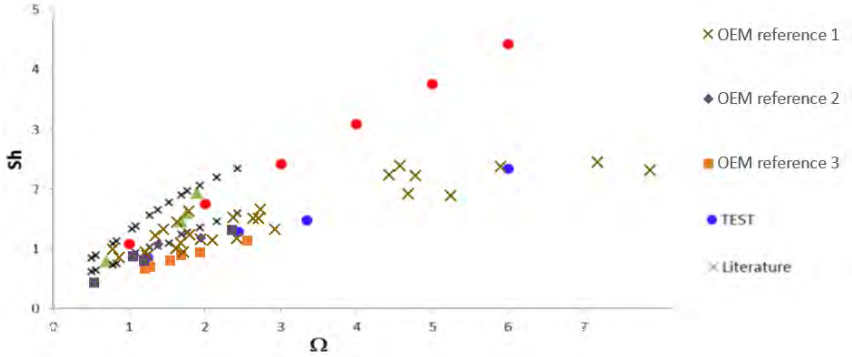


*Figure 30. Strouhal Number in function of the swirl number for the three reference units and for the model test.*

## CONCLUSIONS AND NEXT STEPS

The phenomenon of rotor vibrations induced by vortex flow in expander-generators was characterized, with details on the physical mechanism causing vibrations and on how the operating parameters and the geometry of the expander influence the phenomenon.
Based on this theoretical model, several potential mitigating actions were identified and analyzed in the detail. Experimental data from a set of three case studies was presented, to verify the predictions of the physical model and the effects of the mitigating actions, and to validate the correlations between physical parameters (swirl number, Strouhal number) and severity of the phenomenon (quantified by the subsynchronous vibration amplitude and frequency).
The results of this study show that vortex flow represents a significant potential risk of high vibrations for expander-generators; this risk shall be evaluated and addressed during the design phase, taking actions that were proved to strongly reduce the vibration amplitude.
Presently there is little literature on this physical phenomenon, particularly in the specific area of turboexpanders. Further theoretical and experimental activities are needed to develop a transfer function between the relevant design parameters and the resulting subsynchronous vibration amplitude and frequency; the final purpose would be to identify some parameter that can be easily calculated during the design phase and allows to make accurate numerical predictions of the expected rotor vibration. Reliable calculation tools could also allow to optimize the design and maximize the effectiveness of the solutions proposed in this paper, including the vortex breakers at expander discharge, the wheel geometry and the best control procedure for managing the startup/shutdown transients and the other off-design conditions of the machine.

## NOMENCLATURE

*Acronyms*

| | |
|---|---|
| BPF | Blade Passing Frequency |
| CFD | Computational Fluid Dynamics |
| EG | Expander Generator |
| FFT | Fast Fourier Transform |
| IGV | Inlet Guide Vanes |
| HP | High Pressure |
| HSR | High Speed Rotor |
| LP | Low Pressure |
| LSR | Low Speed Rotor |

*Symbols*

| | | |
|---|---|---|
| $c_{1u}$ | Tangential velocity at the wheel inlet | (L/T) |
| $c_{2u}$ | Tangential velocity at the wheel outlet | (L/T) |
| $D_1$ | Outer wheel diameter | (L) |

| | | |
|---|---|---|
| $D_2$ | Inlet diffuser diameter | (L) |
| $D_{2s}$ | Diameter at the shroud of the wheel outlet | (L) |
| $f$ | Vortex frequency | (1/T) |
| $\dot{m}$ | Mass flowrate | (M/T) |
| $Q_2$ | Volumetric flowrate at diffuser inlet | ($L^3$/T) |
| $K_{2u}$ | Tangential momentum at diffuser inlet | ($ML^2$/T) |
| $r$ | radial distance from rotation axis | (L) |
| $R$ | Radius | (L) |
| $Sh$ | Strouhal number | ( - ) |
| $u_1$ | Wheel peripheral speed measured at diameter $D_1$ | (L) |
| $W$ | Generated power | ($ML^2/T^3$) |
| $\rho_2$ | Gas density at the diffuser inlet | ($M/L^3$) |
| $\Gamma$ | Circulation | ($L^2$/T) |
| $\Omega$ | Swirl number | ( - ) |

## APPENDIX A - DETAILS OF CFD CALCULATION

### *Approach*

The use of CFD in predicting flow behavior is consolidated in the turbomachinery industry. CFD accuracy and consistency in prediction has improved over the years and this tool is now an essential part of the design process. A CFD study allowed to investigate the vortex flow phenomenon and to understand the flow mechanism that may induce subsynchronous vibrations on an EG rotor. Transient analysis was been performed using a commercial CFD code (CFX) an URANS model with SST turbulence model.

### *Domain*

Ideally, the complete turboexpander geometry (inlet section, nozzle, wheel and diffuser) should be included in the CFD domain to reproduce with optimum accuracy the gas flow in the diffuser. On the other hand, considering the heaviness of the computation effort, some simplification had to be done to the model geometry to make the study feasible while maintaining a good accuracy from aerodynamic standpoint (see Figure 31).

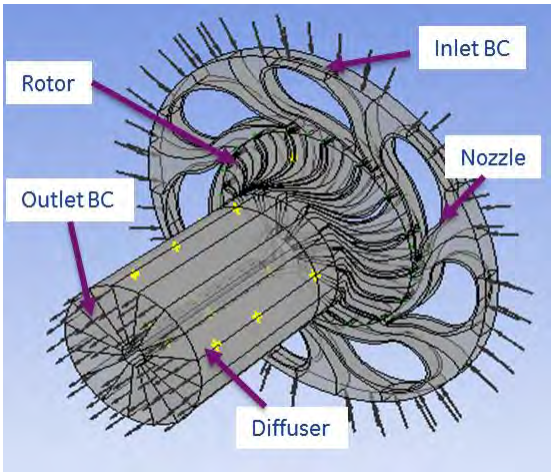


*Figure 31. Calculation domain.*

In the inlet plenum the gas velocity is low and there is no significant flow unsteadiness, therefore this section was not included in the CFD domain; only a small portion immediately adjacent to the IGV nozzles was considered. With a similar approach, the complete conical diffuser was not included but a reasonable length of diffuser is considered in the CFD domain. These two simplifications on the CFD domain definition have negligible impact on the results.

This expander has seven IGV nozzles and 16 wheel blades. It was therefore necessary to model the full wheel instead of a meridional slice. In the current model, rotor and the diffuser are combined in a single mesh to reduce the total number of subdomains and interfaces. A small solid cylindrical section, equivalent to a shaft, was added in the model to improve the mesh quality in proximity of the rotation axis. This modification is not expected to introduce any significant alteration in the development of the vortex flow in the diffuser.

### *Boundary conditions*

Inlet boundary is defined at a section near to nozzle leading edge where the flow has a very low momentum and therefore total and static flow properties are almost the same. Total pressure and static temperature values are imposed at this section, marked as *Inlet BC* in Figure 31. At the outlet section (*Outlet BC*) the average static pressure is imposed. All the walls are defined as adiabatic and wall roughness is not considered in this analysis.

### *Time step and length of analysis*

Since the objective of this study was to analyze flow unsteadiness at subsynchronous frequency, an URANS calculation was carried out for several rotation cycles of the wheel to capture the diffuser vortex flow and its frequency. The number of time steps per wheel rotation and the time step were chosen as a compromise between required frequency resolution and computational time. This resulted in 128 time steps per wheel rotation; no convergence issue was detected. 20+ full wheel revolutions were computed in the whole simulation.

### *Results*

As first step a steady RANS model was run to predict the time-averaged solution for a preselected operating condition, where vortex flow development is expected. The steady solution convergence quality was an important factor for a smooth execution of the URANS

calculation.
RANS calculation confirmed the presence of reverse flow and its penetration inside the diffuser, as reported in Figure 7 where the blue region represents the reverse flow. Once the steady calculation was completed, its solution was used as the initial flow field condition for the URANS calculation.
After a few timesteps, flow parameters started to oscillate around a mean value showing a stable behavior. 18 virtual CFX probes were placed in the diffuser domain to investigate the phenomenon, by extracting and recording static pressure trends during the simulation. These probes are distributed in three sectional planes according to Figure 32.

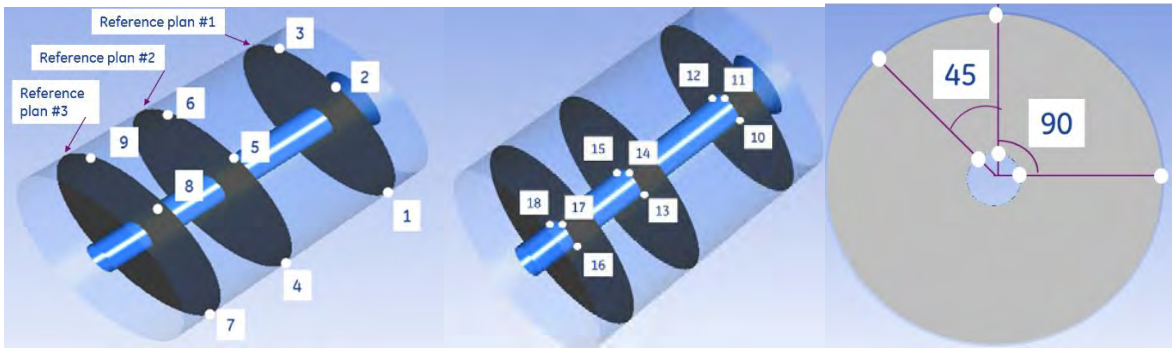


*Figure 32. CFD domain considered for the analysis. Reference planes and probe locations are also reported.*

Figure 8 shows the tridimensional shape of the reverse flow region. This region keeps rotating about the diffuser axis at subsynchronous speed, as described later in this section.
In Figure 33 the static pressure distribution at the middle section in the diffuser (Reference Plane #2 in Figure 32) is plotted for four different time steps. It clearly shows the lobed nature of this phenomenon and its development along the time.

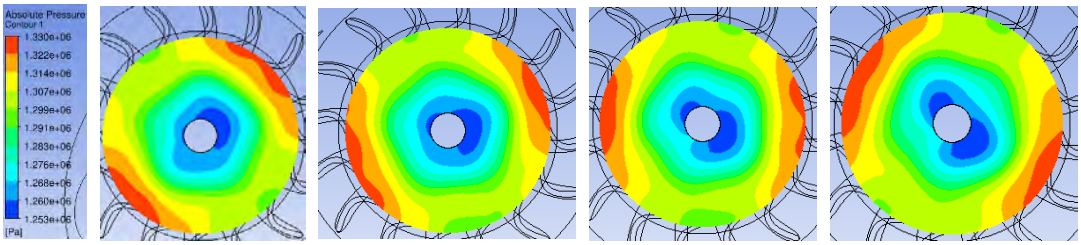

*Figure 33. Static pressure distribution at four different time steps (Reference plane #2).*

The static pressure data captured by the pressure probes were processed by performing a FFT analysis to extract the frequency content, as reported in Figure 34 and 35. These frequency spectra show a clear peak in the subsynchronous region, around 220 Hz (about 80 percent of 1XRev) whose amplitude is comparable with the BPF (Blade Passing Frequency).

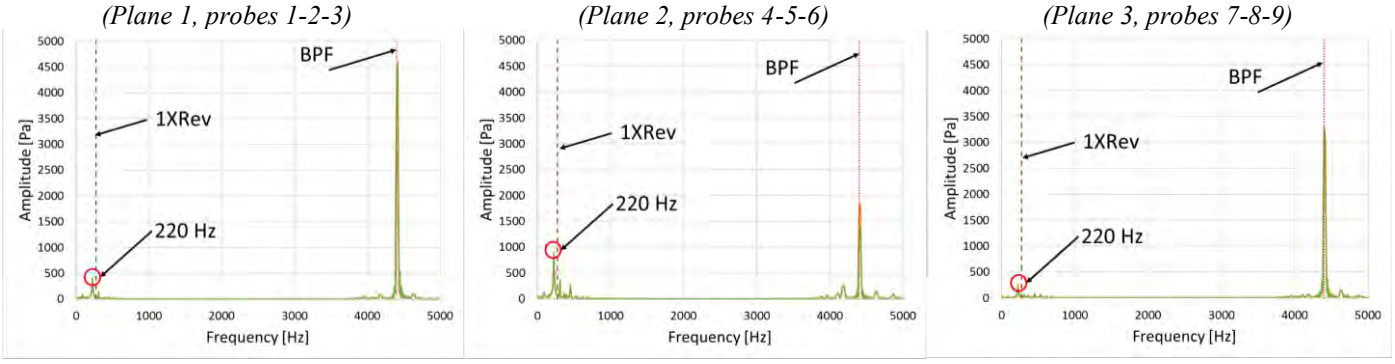


*Figure 34. FFT of pressure data form probes near the diffuser wall.*

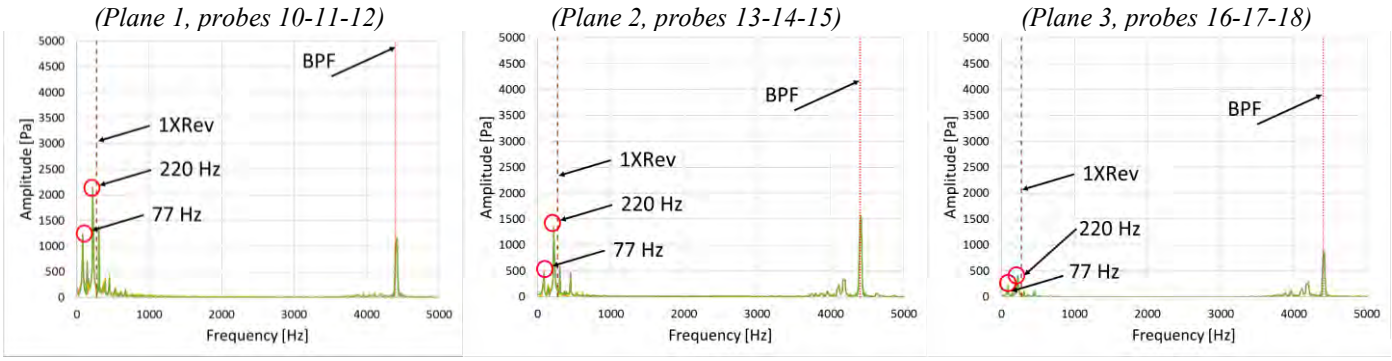


*Figure 35. FFT of pressure data form probes near the axis.*

FFT performed on the probes near the rotation axis (Figure 35) show a lower peak frequency at 77 Hz (28 percent of 1XRev), in line with frequency values reported in literature (Jacob et al., 1996). Figure 36 shows the raw data (time histories) of the three pressure probes located at the same section; a modulation of the signal is clearly visible, with three wavelengths over the period of one wheel rotation cycle. This confirms the presence of three different lobes in the pressure distribution.

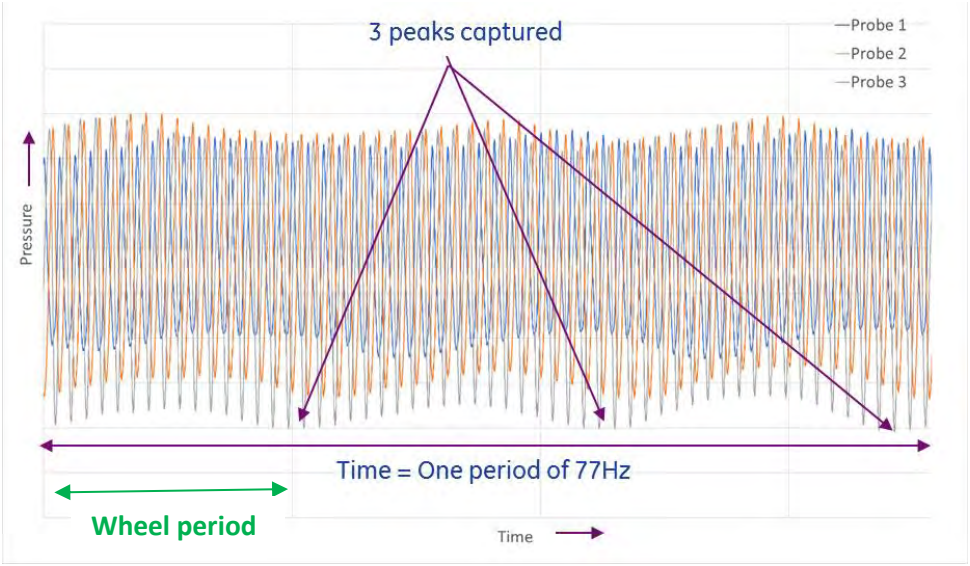


*Figure 36. Static pressure plotted vs. time.*

The results of this analysis confirm that the CFD model is able to reproduce the main features of the vortex flow phenomenon. The rotating pressure gradient predicted by the analysis is a source of excitation for the rotor, that can explain the subsynchronous vibration observed in the case study. Some mismatch is still present with respect to experimental data, mainly in terms of frequency of the subsynchronous peak, and could be reduced by refining the model.

## REFERENCES

Abbott, I. H., Voon Doenhoff, A. E., and Stivers, L. S., 1945, “Summary of Airfoil Data”, Report No. 824, National Advisory Committee For Aeronautics.

Bloch, H. P., and Soares, C., 2001, "Turboexpanders and Process Applications", Gulf Professional Publishing, Woburn, MA.

Cassidy, J. and Falvey, H., 1970, "Observations of Unsteady Flow Arising After Vortex Breakdown", Journal of Fluid Mechanics, 41(04), pp. 727-736.

Falvey, H. and Cassidy, J., 1970, “Frequency and Amplitude of Pressure Surge Generated By Swirling Flow”, Symposium Stockholm

1970, Transaction Part I.

Fiaschi, D., Manfrida, G. and Maraschiello, F., 2015, "Design and performance prediction of radial ORC turboexpanders", Applied Energy, 138, pp. 517-532.

Hirata, D., Nagai, N. and Higashimori, H., 2017, "Subsynchronous Shaft Vibration in an Integrally Geared Expander-Compressor due to Vortex Flow in an Expander", Proceedings of the 46th Turbomachinery Symposium, Turbomachinery Laboratory, Texas A&M University, College Station, TX.

Jacob, T. and Prenat, J.-E., 1996, "Francis Turbine Surge: Discussion and Data Base", Proceedings of the 18th IAHR Symposium, Valencia, Spain.

Kun, L. C., 1987, "Expansion turbines and refrigeration for gas separation and liquefaction", Advances in Cryogenic Engineering, Vol.33, pp. 963-973.

Nishi, M., Yoshida, K., Yano, M., Okamoto, M., Miyagawa, K. and Liu, S., 2007, "A Preliminary Study On The Swirling Flow In A Conical Diffuser With Jet Issued At The Center Of The Inlet", 2nd IAHR International Meeting of the Workgroup on Cavitation and Dynamic Problems in Hydraulic Machinery and Systems, Timisoara, Romania.

Powell, A., 1964, "Theory of vortex sound", The Journal of the acoustical Society of America. Vol. 36, No. 1.

Rohlik, H. E., 1968, "Analytical determination of radial inflow turbine geometry for maximum efficiency", NASA TN D-4384/2, Washington, DC.

Sobey, I. J., 1982, "Oscillatory flows at intermediate Strouhal number in asymmetry channels". Journal of Fluid Mechanics. 125: 359–373.

Tse, M.C., 2004, "Vortex Whistle in Radial Intake", RTO AVT Symposium , Prague, Czech Republic.

Wood, V. T. and White, L. W., 2010, "A New Parametric Model of Vortex Tangential-Wind Profiles: Development, Testing, and Verification", Journal of the Atmospheric Sciences.

Zhang, L. and Jin, Y., 2012, "Numerical Investigation on Vortex Structure and Aerodynamic noise Performance of Small Axial Flow Fan", Journal of Fluid Dynamics, 2, 359-367.